

Structural influence of the length and functionality of *N,N*-donor spacers in Cd(II) ladder-type coordination polymers

Daniel Ejarque^a, Teresa Calvet^b, Mercè Font-Bardia^c, Josefina Pons^{a,*}

^a Departament de Química, Universitat Autònoma de Barcelona, 08193-Bellaterra, Barcelona, Spain

^b Departament de Mineralogia, Petrologia i Geologia Aplicada, Universitat de Barcelona, Martí i Franquès s/n, 08028 Barcelona, Spain

^c Unitat de Difracció de Raig-X, Centres Científics i Tecnològics de la Universitat de Barcelona (CCITUB), Universitat de Barcelona, Solé i Sabaris, 1-3, 08028 Barcelona, Spain



ARTICLE INFO

Article history:

Received 3 December 2022

Revised 27 December 2022

Accepted 31 December 2022

Available online 1 January 2023

Keywords:

Cd(II) compounds

X-ray crystal structure

N,N-donor linkers

Spacer length effect

Ladder-type coordination polymers

Photophysical properties

ABSTRACT

The understanding of the effect generated by small differences of the organic ligands on the molecular and supramolecular arrangement of coordination polymers (CPs) is a key factor to control their properties. Therefore, the study of structurally related ligands differing in some factors *inter alia* functional group orientation, length, or functionality is a crucial task for crystal engineers. In this contribution, the reactions between Cd(OAc)₂·2H₂O, *α*-acetamidocinnamic acid (HACA) and different *N,N*-donor spacers with increasing length (pyrazine, pyz; 4,4'-bipyridine, 4,4'-bipy; 1,2-bis(4-pyridyl)ethylene, 1,2-bpe), as well as additional functionalities (4,4'-azopyridine, 4,4'-azpy) have been successfully performed. Their crystal structures have been elucidated revealing a family of ladder-type 1D CPs showing molecular arrays with single pillars for {[Cd₂(μ-ACA)₂(ACA)₂(pyz)(H₂O)₂]·2EtOH}_n (**1**), and double pillars for [Cd₂(μ-ACA)₂(ACA)₂(4,4'-bipy)₂]_n (**2**), [Cd₂(μ-ACA)₂(ACA)₂(1,2-bpe)₂]_n (**3**) and {[Cd₂(μ-ACA)₂(ACA)₂(4,4'-azpy)₂]·4,4'-azpy·9H₂O}_n (**4**). Remarkably, the effect of the addition of the azo group in **4** compared with **2** and **3** has led to a CP with the same molecular arrangement but different crystal packing, allowing the introduction of one non-coordinated 4,4'-azpy and nine water molecules. Finally, their solid-state UV-Vis and photoluminescence have been measured observing their blue-emitting properties.

© 2022 The Author(s). Published by Elsevier B.V.

This is an open access article under the CC BY license (<http://creativecommons.org/licenses/by/4.0/>)

1. Introduction

The rational design of coordination polymers (CPs) by means of crystal engineering has emerged as a hot topic during the last decades [1–3], providing a tool for chemist to design specific arrangements with potential applications in fluorescence [4,5], magnetism [6,7], or catalysis [8], among others [9,10].

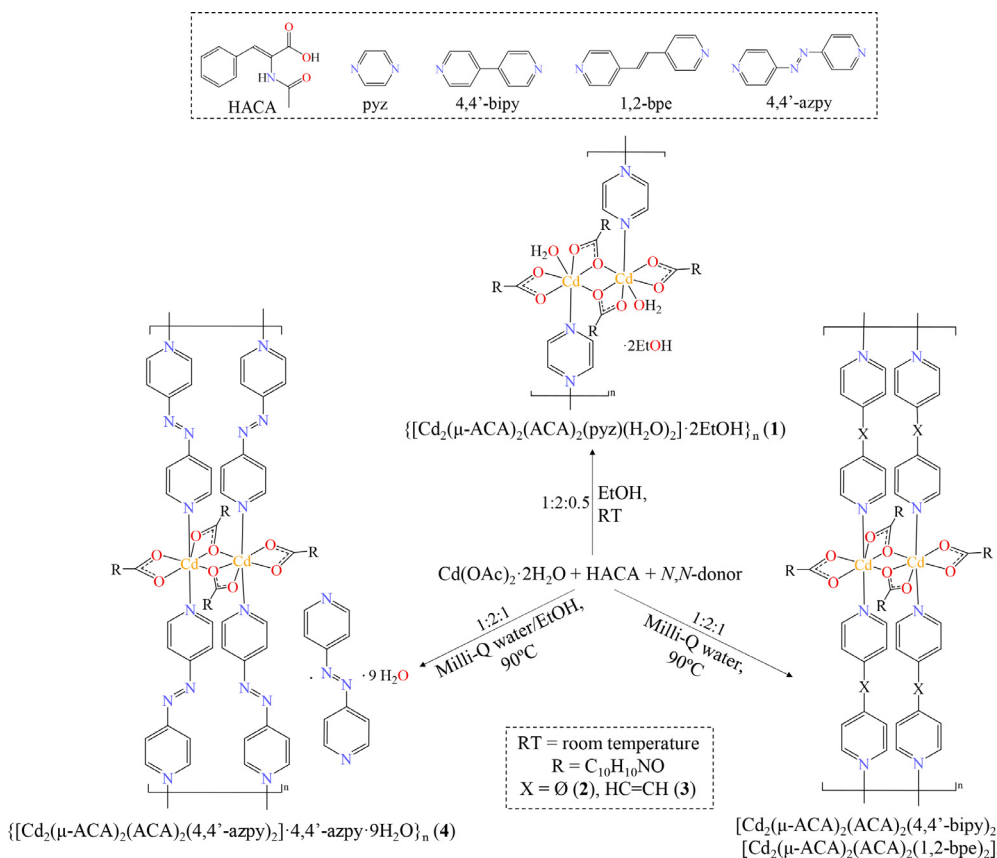
In this context, d¹⁰ metal ions have been specially utilized owing to their close-shell configuration, which provides variable geometries and therefore, structural diversity to the resulting CPs [11,12]. Among them, those presenting bigger ionic radii such Cd(II) offer a wide range of coordination numbers oscillating between two and eight [13]. Their size combined with its relatively high electronegativity compared with the rest of d¹⁰ metal ions [14,15], confers it the possibility to reach a larger number of coordination bonds with more ionic character, which is pursued for

avoiding heavy atom effects in fluorescence materials [16]. However, this structural diversity requires of a precise control of the synthetic conditions such as solvent [17], ratio of reactants [18], or temperature [19], in order to achieve the desired CPs.

In this scenario, the approach consisting on the preparation of CPs with the same molecular arrangement by changing some characteristics of their starting ligands (mainly functional groups and/or ligand lengths) has been successfully employed to prepare diverse families of CPs and studying their properties [20–22]. Nonetheless, these small changes can also influence the structure of CPs leading to the obtention of products with different molecular and/or supramolecular structures [23,24]. Therefore, given our previous experience in the preparation of ACA-based complexes containing Zn(II) and Cd(II) as metal nodes [25–29], in this contribution we have prepared four Cd(II) CPs containing ACA as a common ligand and four different *N,N*-donor spacers (pyrazine, pyz; 4,4'-bipyridine, 4,4'-bipy; 1,2-bis(4-pyridyl)ethylene, 1,2-bpe; 4,4'-azopyridine, 4,4'-azpy) presenting different lengths, ranging from ~2.80 Å to 9.44 Å, as well as an additional functionality in 4,4'-azpy. From the reactions between Cd(OAc)₂·2H₂O,

* Corresponding author.

E-mail address: josefina.pons@uab.es (J. Pons).

**Scheme 1.** Outline of the synthesis of CPs **1-4**.

α -acetamidocinnamic acid (HACA) and the corresponding linkers, we have successfully synthesized four CPs referred as $\{[\text{Cd}_2(\mu\text{-ACA})_2(\text{ACA})_2(\text{pyz})(\text{H}_2\text{O})_2]\cdot 2\text{EtOH}\}_n$ (**1**), $[\text{Cd}_2(\mu\text{-ACA})_2(\text{ACA})_2(4,4'\text{-bipy})_2]_n$ (**2**), $[\text{Cd}_2(\mu\text{-ACA})_2(\text{ACA})_2(1,2\text{-bpe})_2]_n$ (**3**), and $\{[\text{Cd}_2(\mu\text{-ACA})_2(\text{ACA})_2(4,4'\text{-azpy})_2]\cdot 4,4'\text{-azpy}\cdot 9\text{H}_2\text{O}\}_n$ (**4**) (**Scheme 1**). The crystal structures of the four CPs have been elucidated and analyzed. The effects generated by the change in length of the different linkers as well as the introduction of the N=N group in the 4,4'-azpy ligand of **4** have been discussed. Finally, we have studied the solid-state absorption and emission properties of the resulting compounds.

2. Experimental

2.1. Materials and general details

$\text{Cd(OAc)}_2 \cdot 2\text{H}_2\text{O}$, HACA, pyz, 4,4'-bipy, 1,2-bpe, 4,4'-azpy ligands, and acetone, diethyl ether (Et_2O), and ethanol (EtOH) as solvents were purchased from Sigma-Aldrich. All of them were used without further purification. The water used for the preparation of **2-4** was obtained with a Milli-Q® system (18.2 $\text{M}\Omega\cdot\text{cm}$). Deuterated dimethylsulfoxide ($\text{DMSO}-d_6$) was used for the NMR experiments and was purchased from Eurisotop. The reactions and manipulations for the obtention of **1** were carried out at room temperature (RT), while those for the synthesis of **2-4** were done in a Digiheat-TFT furnace (JP Selecta) using sealed vials under autogenous pressure, and a cooling ramp from 90 °C to RT (SI: Fig. S1). Powder X-ray diffraction (PXRD) patterns were measured with a Panalytical X'pert PRO MPD apparatus using a monochromatic $\text{CuK}\alpha$ radiation with $\lambda = 1.5406 \text{ \AA}$. All of them were recorded from $2\theta = 5^\circ$ to 30° with a step scan of 0.01671°. Elemental analyses (EA) were

carried on a Thermo Scientific Flash 2000 CHNS Analyzer. FTIR-ATR spectra were recorded on a Perkin Elmer spectrometer, equipped with an attenuated total reflectance (ATR) accessory model MKII Golden Gate with diamond window in the range 4000–500 cm^{-1} . ^1H , $^{13}\text{C}[^1\text{H}]$ and DEPT-135 NMR spectra were recorded on a Bruker Ascend 300 MHz spectrometer in $\text{DMSO}-d_6$ solutions at RT. All the chemical shifts (δ) are given in ppm relative to tetramethylsilane (Me_4Si) as internal standard. Solid-state UV-Vis spectra were carried out using a Cary 4000 spectrophotometer between 200–800 nm. Solid-state photoluminescence measurements were recorded using a Varian Cary Eclipse Fluorescence spectrophotometer. CIE 1931 chromaticity diagram was generated using Origin Pro 2019b software.

2.2. Synthesis of compound 1

An EtOH solution (8 mL) of $\text{Cd(OAc)}_2 \cdot 2\text{H}_2\text{O}$ (100 mg, 0.375 mmol) was added dropwise to an EtOH solution (10 mL) of HACA (156 mg, 0.760 mmol) and pyz (15.1 mg, 0.189 mmol) at RT. The solution was stirred during 24 h, and then it was kept evaporating at RT during 10 days until a white crystalline solid precipitated. The resulting product was filtered, washed with 10 mL of cold Et_2O (repeated twice), and dried under vacuum. Single crystals suitable for X-ray diffraction were obtained after layering 2 mL of hexane above 2 mL of a solution of the reaction mixture and kept it undisturbed at RT for four days.

1. Yield: 167 mg (71.2%) (based on Cd). Elemental analysis calc. (%) for $\text{C}_{52}\text{H}_{60}\text{Cd}_2\text{N}_6\text{O}_{16}$ (1249.88): C 49.97; H 4.84; N 6.72; found: C 49.74; H 4.72; N 6.55. FTIR-ATR (wavenumber, cm^{-1}): 3355(w) [$\nu(\text{O-H})$], 3249(m) [$\nu(\text{N-H})$], 3168–3024(br) [$\nu(\text{C-H})_{\text{ar}} + \nu(\text{C-H})_{\text{alk}}$], 2982–2934(br) [$\nu(\text{C-H})_{\text{alp}}$], 1677(w), 1663(w), 1648(m) [$\nu(\text{C=O})$],

1549(w) [$\nu(C=C/C=N)$], 1516(s) [$\nu_{as}(COO)$], 1492(m), 1446(w), 1416(s) [$\nu_s(COO)$], 1399(s) [$\delta(C=C/C=N)$], 1370(s) [$\nu_s(COO)$], 1357(s) [$\delta(C=C/C=N)$], 1279(m), 1212(w), 1185(w), 1159(w), 1128(w), 1110(w), 1083(w), 1059(w), 1047(m) [$\delta_{ip}(C-H)$], 1031(w), 1004(w), 984(w), 974(w), 943(w), 918(w), 893(w), 877(w), 856(w), 846(w), 813(w), 788(w), 780(w), 766(m) [$\delta_{oop}(C-H)$], 752(w), 727(w), 690(s) [$\delta_{oop}(C-H)$], 597(m), 565(m), 545(m), 518(s). 1H NMR (300 MHz; DMSO- d_6 ; Me₄Si; 298 K): δ = 9.17 [4H, s, NH_{ACA}], 8.66 [4H, s, H_{pyz}], 7.50 [8H, d, 3J = 7.2 Hz, o-H_{ACA}], 7.35 [8H, t, 3J = 7.5 Hz, m-H_{ACA}], 7.27 [8H, m, p-H_{ACA} + NH-C-H_{ACA}], 4.34 [2H, t, 3J = 5.1 Hz, OH_{EtOH}], 3.44 [4H, qd, 3J = 7.0 Hz, 4J = 5.1 Hz, CH_{2-EtOH}], 1.96 [12H, s, CO-CH_{3,ACA}], 1.05 [6H, t, 3J = 7.0 Hz, CH_{3-EtOH}]. $^{13}C\{^1H\}$ NMR (75 MHz; DMSO- d_6 ; Me₄Si; 298 K): δ = 171.5 [NH-CO_{ACA}], 168.1 [COO_{ACA}], 145.2 [C_{pyz}], 135.2 [O₂C-_{ACA}], 129.5 [HN-C-CH-C_{ACA}], 129.3 [o-C_{ACA}], 129.0 [p-C_{ACA}], 128.2 [m-C_{ACA}], 128.0 [NH-C-CH-C_{ACA}], 56.0 [CH_{2-EtOH}], 23.0 [CO-CH_{3,ACA}], 18.6 [CH_{3-EtOH}]. DEPT-135 NMR (75 MHz; DMSO- d_6 ; Me₄Si; 298 K): δ = 145.2 [C_{pyz}], 129.2 [o-C_{ACA}], 128.9 [p-C_{ACA}], 128.2 [m-C_{ACA}], 128.0 [NH-C-CH-C_{ACA}], 56.0 [CH_{2-EtOH}], 23.0 [CO-CH_{3,ACA}], 18.5 [CH_{3-EtOH}]. UV-Vis: $\lambda_{max-Abs}$ = 252, 302 nm. Fluorescence: λ_{exc} = 262 nm $\rightarrow \lambda_{em}$ = 359, 422, 491 nm; λ_{exc} = 315 nm $\rightarrow \lambda_{em}$ = 360, 376, 392 nm.

2.3. Synthesis of compounds 2-4

For **2** and **3**, a hot Milli-Q water solution (1.0 mL, **2**; 3.0 mL, **3**) of Cd(OAc)₂·2H₂O (50.0 mg, 0.188 mmol) was added dropwise to a hot Milli-Q water solution (4.0 mL) of HACA (77.0 mg, 0.375 mmol) and 0.188 mmol of the corresponding *N,N*-donor spacer (4,4'-bipy, **2**; 1,2-bpe, **3**). The preparation of **4** was done using the same molar ratio as for **2** and **3** but starting from 0.5 mL of a hot Milli-Q water solution of Cd(OAc)₂·2H₂O (10 mg, 0.038 mmol), and a hot solution of Milli-Q water/EtOH (1.25 mL/25.0 μ L) with the ligands. The resulting solutions of **2-4** were kept at 90 °C during 2 h and then, they were cooled down to RT using a temperature ramp (SI: Fig. S1), obtaining single crystals suitable for X-ray diffraction when the cooling ramp was completed for **2** and **3**, while the single crystals of **4** were obtained after keeping the vials undisturbed at RT for three days once the cooling ramp was completed. All the crystals were filtered, washed twice with 5 mL of acetone, and dried under vacuum.

2. Yield: 99.3 mg (78.2%) (based on Cd). Elemental analysis calc. (%) for C₆₄H₅₆Cd₂N₈O₁₂ (1354.00): C 56.77; H 4.17; N 8.28; found: C 56.62; H 4.02; N 8.39. FTIR-ATR (wavenumber, cm⁻¹): 3410(w) [$\nu(N-H)$], 3090-3060(br) [$\nu(C-H)_{ar}$ + $\nu(C-H)_{alk}$], 2983-2874(br) [$\nu(C-H)_{al}$], 1687(w), 1660(s) [$\nu(C=O)$], 1641(sh), 1604(m), 1554(s) [$\nu(C=C/C=N)$], 1543(s) [$\nu_{as}(COO)$], 1492(w) [$\nu_{as}(COO)$], 1477(w), 1448(w), 1415(sh), 1388(s) [$\nu_s(COO)$], 1349(s) [$\delta(C=C/C=N)$], 1329(s), 1255(m), 1223(m), 1184(w), 1162(w), 1125(w), 1077(m) [$\delta_{ip}(C-H)$], 1044(w), 1033(w), 1012(w), 967(w), 935(w), 864(w), 855(w), 821(m), 792(m), 771(s) [$\delta_{oop}(C-H)$], 746(m), 733(m), 690(s) [$\delta_{oop}(C-H)$], 675(w), 662(w), 632(m), 597(sh), 589(w), 574(w), 543(sh), 531(w), 521(sh). 1H NMR (300 MHz; DMSO- d_6 ; Me₄Si; 298 K): δ = 9.18 [4H, s, NH_{ACA}], 8.73 [8H, d, 3J = 4.1 Hz, o-H_{4,4'-bipy}], 7.84 [8H, d, 3J = 4.1 Hz, m-H_{4,4'-bipy}], 7.50 [8H, d, 3J = 6.8 Hz, o-H_{ACA}], 7.35 [8H, t, 3J = 7.1 Hz, m-H_{ACA}], 7.28 [8H, m, p-H_{ACA} + NH-C-H_{ACA}], 1.96 [12H, s, CO-CH_{3,ACA}]. $^{13}C\{^1H\}$ NMR (75 MHz; DMSO- d_6 ; Me₄Si; 298 K): δ = 171.3 [NH-CO_{ACA}], 168.2 [COO_{ACA}], 150.6 [o-C_{4,4'-bipy}], 144.4 [N-CH-CH-C_{4,4'-bipy}], 135.2 [O₂C-_{ACA}], 129.5 [HN-C-CH-C_{ACA}], 129.3 [o-C_{ACA}], 128.9 [p-C_{ACA}], 128.3 [m-C_{ACA}], 128.1 [NH-C-CH-C_{ACA}], 121.3 [m-C_{4,4'-bipy}], 23.0 [CO-CH_{3,ACA}]. DEPT-135 NMR (75 MHz; DMSO- d_6 ; Me₄Si; 298 K): δ = 150.6 [o-C_{4,4'-bipy}], 129.3 [o-C_{ACA}], 128.9 [p-C_{ACA}], 128.3 [m-C_{ACA}], 128.1 [NH-C-CH-C_{ACA}], 121.3 [m-C_{4,4'-bipy}], 23.0 [CO-CH_{3,ACA}]. UV-Vis: $\lambda_{max-Abs}$ = 264, 290 nm. Fluorescence: λ_{exc} = 262

nm $\rightarrow \lambda_{em}$ = 358, 422, 491 nm; λ_{exc} = 315 nm $\rightarrow \lambda_{em}$ = 361, 377, 392 nm.

3. Yield: 85.7 mg (65.0%) (based on Cd). Elemental analysis calc. (%) for C₆₈H₆₀Cd₂N₈O₁₂ (1406.07): C 58.09; H 4.30; N 7.97; found: C 57.86; H 4.18; N 7.72. FTIR-ATR (wavenumber, cm⁻¹): 3402(w) [$\nu(N-H)$], 3062-3028(br) [$\nu(C-H)_{ar}$ + $\nu(C-H)_{alk}$], 2985-2941(br) [$\nu(C-H)_{al}$], 1686(w), 1661(m) [$\nu(C=O)$], 1640(w), 1609(m), 1563(sh) [$\nu(C=C/C=N)$], 1547(s) [$\nu_{as}(COO)$], 1484(w) [$\nu_{as}(COO)$], 1445(w), 1429(w), 1387(s) [$\nu_s(COO)$], 1362(sh) [$\delta(C=C/C=N)$], 1332(m), 1309(m), 1255(m), 1221(sh), 1209(w), 1181(w), 1157(w), 1120(w), 1101(m), 1077(w), 1073(w), 1017(m) [$\delta_{ip}(C-H)$], 1002(w), 960(w), 936(w), 842(m), 793(w), 771(m) [$\delta_{oop}(C-H)$], 740(m), 692(s) [$\delta_{oop}(C-H)$], 588(w), 552(s), 534(s). 1H NMR (300 MHz; DMSO- d_6 ; Me₄Si; 298 K): δ = 9.18 [2H, s, NH_{ACA}], 8.61 [4H, d, 3J = 5.7 Hz, o-H_{1,2-bpe}], 7.62 [4H, dd, 3J = 4.1 Hz, 4J = 1.5 Hz, m-H_{1,2-bpe}], 7.55 [2H, s, py-CH_{1,2-bpe}], 7.50 [4H, d, 3J = 7.3 Hz, o-H_{ACA}], 7.35 [4H, t, 3J = 7.3 Hz, m-H_{ACA}], 7.27 [4H, m, p-H_{ACA} + NH-C-H_{ACA}], 1.96 [6H, s, CO-CH_{3,ACA}]. $^{13}C\{^1H\}$ NMR (75 MHz; DMSO- d_6 ; Me₄Si; 298 K): δ = 171.3 [NH-CO_{ACA}], 168.2 [COO_{ACA}], 150.2 [o-C_{1,2-bpe}], 143.5 [N-CH-CH-C_{1,2-bpe}], 135.1 [O₂C-_{ACA}], 130.7 [py-CH_{1,2-bpe}], 129.5 [HN-C-CH-C_{ACA}], 129.3 [o-C_{ACA}], 129.0 [p-C_{ACA}], 128.3 [m-C_{ACA}], 128.1 [NH-C-CH-C_{ACA}], 121.4 [m-C_{1,2-bpe}], 23.0 [CO-CH_{3,ACA}]. DEPT-135 NMR (75 MHz; DMSO- d_6 ; Me₄Si; 298 K): δ = 150.2 [o-C_{1,2-bpe}], 130.6 [py-CH_{1,2-bpe}], 129.3 [o-C_{ACA}], 128.9 [p-C_{ACA}], 128.2 [m-C_{ACA}], 128.1 [NH-C-CH-C_{ACA}], 121.3 [m-C_{1,2-bpe}], 23.0 [CO-CH_{3,ACA}]. UV-Vis: $\lambda_{max-Abs}$ = 276, 329 nm. Fluorescence: λ_{exc} = 262 nm $\rightarrow \lambda_{em}$ = 360, 421, 492 nm; λ_{exc} = 315 nm $\rightarrow \lambda_{em}$ = 362, 377, 391 nm.

4. Yield: 12.2 mg (55.6%) (based on 4,4'-azpy). Elemental analysis calc. (%) for C₇₄H₈₂Cd₂N₁₆O₂₁ (1756.36): C 50.60; H 4.71; N 12.76; found: C 50.84; H 4.49; N 12.91. FTIR-ATR (wavenumber, cm⁻¹): 3389-2639(br) [$\nu(O-H)+\nu(N-H)+\nu(C-H)$], 1670(sh), 1655(w) [$\nu(C=O)$], 1645(w), 1598(w), 1567(sh) [$\nu(C=C/C=N)$], 1544(s) [$\nu_{as}(COO)$], 1536(s), 1527(s) [$\nu_{as}(COO)$], 1513(sh), 1492(m), 1446(w), 1398(s) [$\nu_s(COO)$], 1364(s) [$\delta(C=C/C=N)$], 1325(sh), 1285(w), 1224(w), 1212(w), 1185(w), 1140(w), 1123(w), 1081 (w), 1051(w), 1030(w), 1016(m) [$\delta_{ip}(C-H)$], 983(w), 964(w), 929(w), 917(w), 842(w), 784(w), 775(m) [$\delta_{oop}(C-H)$], 744(w), 693(m) [$\delta_{oop}(C-H)$], 608(w), 593(w), 567(m), 544(w), 524(m). 1H NMR (300 MHz; DMSO- d_6 ; Me₄Si; 298 K): δ = 9.15 [4H, s, NH_{ACA}], 8.88 [12H, dd, 3J = 4.6 Hz, 4J = 1.4 Hz, o-H_{4,4'-azpy}], 7.81 [12H, dd, 3J = 4.6 Hz, 4J = 1.5 Hz, m-H_{4,4'-bipy}], 7.48 [8H, d, 3J = 7.0 Hz, o-H_{ACA}], 7.34 [8H, t, 3J = 7.3 Hz, m-H_{ACA}], 7.27 [4H, d, p-H_{ACA}], 3J = 7.2 Hz], 7.25 [4H, s, NH-C-H_{ACA}], 1.95 [12H, s, CO-CH_{3,ACA}]. $^{13}C\{^1H\}$ NMR (75 MHz; DMSO- d_6 ; Me₄Si; 298 K): δ = 171.4 [NH-CO_{ACA}], 168.2 [COO_{ACA}], 156.4 [N-CH-CH-C_{4,4'-azpy}], 151.9 [o-C_{4,4'-azpy}], 135.2 [O₂C-_{ACA}], 129.6 [HN-C-CH-C_{ACA}], 129.4 [o-C_{ACA}], 129.1 [p-C_{ACA}], 128.4 [m-C_{ACA}], 128.2 [NH-C-CH-C_{ACA}], 116.2 [m-C_{4,4'-azpy}], 23.1 [CO-CH_{3,ACA}]. DEPT-135 NMR (75 MHz; DMSO- d_6 ; Me₄Si; 298 K): δ = 151.9 [o-C_{4,4'-azpy}], 129.4 [o-C_{ACA}], 129.1 [p-C_{ACA}], 128.4 [m-C_{ACA}], 128.2 [NH-C-CH-C_{ACA}], 116.2 [m-C_{4,4'-azpy}], 23.1 [CO-CH_{3,ACA}]. UV-Vis: $\lambda_{max-Abs}$ = 285, 345, 470 nm. Fluorescence: λ_{exc} = 262 nm $\rightarrow \lambda_{em}$ = 359, 422, 493 nm; λ_{exc} = 315 nm $\rightarrow \lambda_{em}$ = 374, 386 nm; λ_{exc} = 470 nm $\rightarrow \lambda_{em}$ = 484 nm.

2.4. X-ray crystallographic data

Colorless (**1-3**) and red-prism (**4**) specimens were used for the X-ray crystallographic analysis. The X-ray intensity data were measured on a D8 Venture system equipped with a multilayer monochromator and a Mo microfocus (λ = 0.71073 Å). For all the compounds, the frames were integrated using the Bruker SAINT software package using a narrow-frame algorithm. The structures were solved and refined using a SHELXTL Software Package (version-2018/3) [30]. The integration of the data with a 0.80 Å (**1**), 0.68 Å (**2**), 0.79 Å (**3**) and 0.73 Å (**4**) resolution, gave an av-

Table 1
Crystal data and structure refinement for **1–4**.

	1	2	3	4
Empirical Formula	C ₂₆ H ₃₀ CdN ₃ O ₈	C ₃₂ H ₂₈ CdN ₄ O ₆	C ₃₄ H ₃₀ CdN ₄ O ₆	C ₇₄ H ₈₂ Cd ₂ N ₁₆ O ₂₁
Formula weight	624.93	676.98	703.02	1756.35
T (K)	100(2)	100(2)	100(2)	100(2)
Wavelength (Å)	0.71073	0.71073	0.71073	0.71073
System, space group	Monoclinic, P2 ₁ /c	Triclinic, PT	Triclinic, PT	Monoclinic, P2 ₁
Unit cell dimensions				
a (Å)	20.080(3)	10.770(2)	10.396(4)	13.6110(5)
b (Å)	8.5048(13)	10.957(2)	11.761(5)	22.8777(11)
c (Å)	15.726(2)	13.512(3)	13.096(6)	14.3548(7)
α (°)	90	87.154(7)	91.794(14)	90
β (°)	101.199(5)	86.938(7)	92.560(15)	117.209(2)
γ (°)	90	65.068(7)	102.342(15)	90
V (Å ³)	2634.5(7)	1443.2(5)	1561.3(12)	3975.3(3)
Z	4	2	2	2
D _{calc} (mg/m ³)	1.576	1.558	1.495	1.467
μ (mm ⁻¹)	0.883	0.809	0.751	0.617
F (000)	1276	688	716	1804
Crystal size (mm ⁻³)	0.043 × 0.036 × 0.016	0.269 × 0.046 × 0.044	0.134 × 0.029 × 0.012	0.253 × 0.038 × 0.033
hkl ranges	-23 <= h <= 25, -10 <= k <= 10, -19 <= l <= 19	-15 <= h <= 15, -15 <= k <= 15, 0 <= l <= 19	-13 <= h <= 13, -14 <= k <= 14, 0 <= l <= 16	-18 <= h <= 17, -31 <= k <= 31, -19 <= l <= 19
θ range (°)	2.068 to 26.461	2.051 to 31.307	2.008 to 26.696	1.595 to 29.217
Reflections collected/unique/[R _{int}]	20116/5415/0.1824	8914/8914/0.0906	6441/6441/0.1488	149152/21525/0.0718
Completeness to θ (%)	99.9	99.1	99.3	100.0
Absorption correction	Semi-empirical from equivalents	Semi-empirical from equivalents	Semi-empirical from equivalents	Semi-empirical from equivalents
Max. and min. transmission	0.7454 and 0.5210	0.7461 and 0.5441	0.7454 and 0.5717	0.7458 and 0.6510
Refinement method	Full-matrix	Full-matrix	Full-matrix	Full-matrix
Data/Restraints/Parameters	least-squares on F ²			
Goodness-on-fit on F ²	5415/0/322	8914/4/390	6441/0/408	21525/9/1077
Final R indices [I > 2σ(I)]	R ₁ = 0.1060, wR ₂ = 0.1831	R ₁ = 0.0358, wR ₂ = 0.0659	R ₁ = 0.0546, wR ₂ = 0.0910	R ₁ = 0.0357, wR ₂ = 0.0805
R indices (all data)	R ₁ = 0.1691, wR ₂ = 0.2082	R ₁ = 0.0590, wR ₂ = 0.0703	R ₁ = 0.0969, wR ₂ = 0.1012	R ₁ = 0.0409, wR ₂ = 0.0832
Extinction coefficient	n/a	n/a	n/a	n/a
Largest diff-peak and hole (e. Å ⁻³)	1.693 and -1.811	3.060 and -1.105	1.387 and -1.059	1.933 and -0.649

verage redundancy of 3.715 (**1**), 1.000 (**2**), 1.000 (**3**) and 6.929 (**4**), a completeness of 99.6% (**1**), 94.6% (**2**), 97.5% (**3**) and 99.9% (**4**), R_{sig} of 19.19% (**1**), 12.44% (**2**), 15.48% (**3**), and 4.20% (**4**), presenting 3325 (61.40%) (**1**), 6305 (70.73%) (**2**), 4066 (63.13%) (**3**), and 20027 (93.04%) (**4**) reflections greater than 2σ(|F|²).

For **1–4** the final cell constants and volume are based upon refinement of the XYZ-centroids of reflections above 20 σ(I). Data were corrected for absorption effects using the Multi-Scan method (SADABS). Crystal data and additional details of structure refinement for **1–4** are reported in Table 1. Complete information about the crystal structure and molecular geometry is available in CIF format via CCDC 2222663 (**1**), 2222662 (**2**), 2222664 (**3**), and 2222665 (**4**).

Molecular graphics were generated using Mercury 4.3.1 software [31], with the POV-Ray image package [32], and Olex2 software [33]. The color codes for all the molecular graphics are as follows: light orange (Cd), red (O), light blue (N), gray (C), and white (H). All the accessible void volumes have been calculated with Mercury 4.3.1 software [31], using a probe radius of 1.2 Å [34]. The evaluation of the geometry distortion of the Cd(II) cores in **1–4** has been done using version 2.1 of SHAPE software from the corresponding CIF files [35]. The resulting topologies were analyzed with the ToposPro 5.3.3.4 and Gavrog Systre (version 1.2.0 beta2) programs and the TopCryst website (<https://topcryst.com>).

3. Results and discussion

3.1. Preparation of 1–4

The four CPs were prepared from the reaction of Cd(OAc)₂·2H₂O, HACA and their corresponding N,N-donor spacer

(pyz, **1**; 4,4'-bipy, **2**; 1,2-bpe, **3**; 4,4'-azpy, **4**). All the CPs were obtained as crystalline materials, which were used for the further characterization and photophysical properties measurements. Compound **1** was prepared using a 1:2:0.5 molar ratio in EtOH at RT. Otherwise, compounds **2–4** were obtained using a 1:2:1 molar ratio and Milli-Q water, starting the reactions at 90 °C and following a cooling ramp (SI: Fig. S1). Interestingly, the addition of a 1.7% of EtOH to the reaction media in **4** results in a remarkable enhancement of the quality of the crystals. Furthermore, all the assays for obtaining **1** using the same synthetic conditions as for the obtention of **2–4** yielded the monomer [Cd(ACA)₂(H₂O)₂] [25] independently of the utilized stoichiometry. Otherwise, the use of EtOH resulted in the obtention of **1**, and the increase of equivalents of pyz lead to the same product with lower yields.

3.2. General characterization

Compounds **1–4** were characterized by PXRD, EA, FTIR-ATR, ¹H, ¹³C{¹H}, DEPT-135 NMR spectroscopies, and single crystal X-ray diffraction method. Phase purity of the bulk samples of **1–4** were verified by PXRD (SI: Figs. S2–S5). Moreover, the EA agree with the proposed formulas. In the FTIR-ATR spectra we observe the bands attributable to the ACA and N,N-donor spacers. The absence of a strong band at 1637 cm⁻¹ corresponding to ν(COOH)_{HACA} indicates that the HACA ligand is deprotonated in all the CPs. The four spectra display the characteristic bands between 1547–1484 cm⁻¹ for ν_{as}(COO) and 1416–1370 cm⁻¹ for ν_s(COO), whose difference results in the Δ value [36,37], being 146 and 100 cm⁻¹ (**1**), 155 and 104 cm⁻¹ (**2**), 160 and 97 cm⁻¹ (**3**), and 146 and 129 cm⁻¹ (**4**), which suggest bidentate bridged-chelated ($\mu_2\text{-}\eta^1:\eta^1$), and chelated

($\mu_2\text{-}\eta^2$) coordination modes of the carboxylate groups. Additionally, other bands of the ACA corresponding to the $\nu(\text{N-H})$ and $\nu(\text{C=O})$ signals have also been identified, as well as the typical bands from the aromatic rings ($\nu(\text{C=C/C=N})$ and $\delta(\text{C=C/C=N})$) from either ACA and the corresponding spacers [38]. Furthermore, the presence of a broad band between 3355–2862 cm⁻¹ (**1**) and 3389–1639 cm⁻¹ (**4**) has been attributed to $\nu(\text{O-H})$ of solvent molecules (SI: Figs. S6–S9).

The ¹H NMR spectra of **1–4** were recorded in DMSO-*d*₆ solutions to ascertain the molar ratio between the ligands (SI: Figs. S10–S13). All the spectra display a signal between 9.18–9.15 ppm attributable to the amide H-atom, while the signals corresponding to the *N,N*-donor spacers appeared at 8.66 (**1**), 8.73 and 7.84 (**2**), 8.61–7.55 (**3**), and 8.88 and 7.81 (**4**). In addition, the aromatic and the alkene hydrogen atoms from ACA are found between 7.50–7.25 ppm, while the methyl H-atoms are shown around 1.95 ppm. The ¹H NMR spectra of the four CPs confirm their different ACA:spacer ratio, being 4:1 (**1**), 4:2 (**2** and **3**), and 4:3 (**4**), which is in agreement with the elucidated crystal structures [38].

The ¹³C(¹H) and DEPT-135 NMR spectra of **1–4** have also been recorded using DMSO-*d*₆ as solvent, observing the typical signals corresponding to the carbonyl (171.5–171.3 ppm) and carboxylate (168.2–168.1 ppm) carbon atoms from ACA in the downfield region, followed by the carbon atoms from the *N,N*-donor linkers, which appeared between 151.9 and 130.7 ppm. In this region, the aromatic and alkene carbon atoms from ACA are also shown between 135.2 and 128.9 ppm, while the methyl carbon atoms from ACA appeared in the up-field region of the spectra around 23.0 ppm (SI: Figs. S14–S17).

3.3. Crystal and extended structure of complex **1**

The compound belongs to the monoclinic P₂/*c* space group. It consists of a 1D zig-zag CP expanded along the [010] direction through dimeric secondary building units (SBUs) connected by a pyz linker acting as a single pillar (Fig. 1a). These SBUs are formed by two equivalent Cd(II) centers with [CdO₆N] cores connected by two ACA ligands presenting a $\mu_2\text{-}\eta^1\text{:}\eta^1$ coordination mode. In addition, a pair of $\mu_2\text{-}\eta^2$ ACA, a water and a pyz molecules complete the coordination sphere of both Cd(II) centers, displaying a distorted capped trigonal prismatic geometry (Fig. 1b; SI: Table S1).

The crystal structure also contains two equivalent non-coordinated EtOH molecules, which are placed on voids with an accessible volume of 48.61 Å³ (1.8% of the unit cell volume) [34] generated by the supramolecular scaffold of the CP. In addition, their bond lengths and bond angles oscillate between 2.279(8)–2.451(8) Å and 54.9(2)–159.9(3)°, showing similar values than other Cd(II) ladder-type CPs presenting pyz ligands as single pillars (Table 2) [39,40].

The intramolecular interactions of **1** are based on a C-H···O interaction between an *o*-H from pyz and a carboxylate oxygen atom from the $\mu_2\text{-}\eta^2$ ACA ligands (Fig. 1a). The intermolecular interactions form 2D layers along the (200) plane (Fig. 1c) resulting in a hxl topology. This layers are mainly originated by the coordinated water molecules that joint together the polymeric chains, forming two H-bonds with one oxygen atom from the $\mu_2\text{-}\eta^1\text{:}\eta^1$ ACA ligand and one oxygen atom from the $\mu_2\text{-}\eta^2$ carboxylate group as acceptors. The 2D plane is also supported by H-bonds promoted by the NH and C=O groups from the amide moieties from ACA, which interact with nearby $\mu_2\text{-}\eta^1\text{:}\eta^1$ linked oxygen atoms from carboxylate ACA ligands and non-coordinated EtOH molecules, as well as C-H···π interactions involving the EtOH molecules and the polymeric chains (Fig. 1d).

3.4. Crystal structure of complexes **2–4**

Compounds **2–4** belong to the triclinic P₁ (**2**, **3**) and monoclinic P₂ (**4**) space groups. They consist of 1D ladder-type CPs expanded along the [110] (**2**), [220] (**3**) and [100] (**4**) directions (Figs. 2a–c), which are formed by dimeric SBUs connected by double pillars of 4,4'-bipy (**2**), 1,2-bpe (**3**) and 4,4'-azpy (**4**) linkers, showing different degrees of distortion between the pyridyl rings of their corresponding spacers (Figs. 2d–e). Remarkably, compound **4** contains one non-coordinated 4,4'-azpy and nine water molecules located in voids of 257.56 Å³ (6.5% of the unit cell) [34], generated by their supramolecular scaffold along the [100] direction. The three CPs present the same SBU formed by two $\mu_2\text{-}\eta^1\text{:}\eta^1$ ACA ligands joining the metal nodes and two $\mu_2\text{-}\eta^2$ ACA ligands, that combined with two linkers per metal ion form [CdO₅N₂] cores, presenting distorted pentagonal bipyramidal geometries (SI: Table S1). Moreover, the bond lengths and bond angles range be-

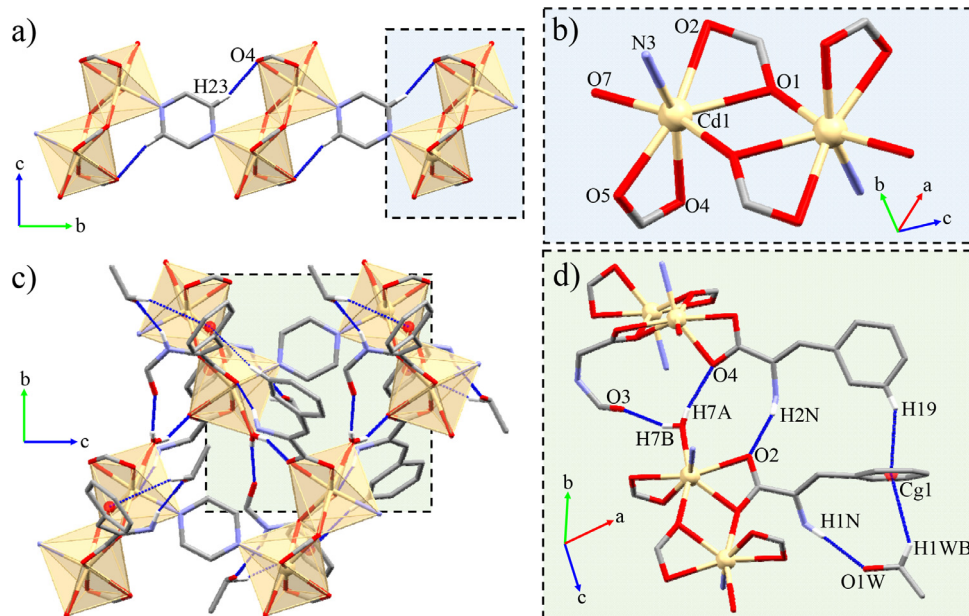


Fig. 1. (a) Molecular structure of compound **1**. (b) Dimeric SBU. (c) General and (d) In detail views of the intermolecular interactions expanding the structure through the (200) plane. All the atoms not involved in the highlighted interactions have been omitted for clarity.

Table 2
Selected bond lengths (\AA), bond angles ($^\circ$), intra- and intermolecular interactions (\AA) for **1**.

Bond lengths (\AA)					
Cd(1)-O(1)	2.339(7)	Cd(1)-O(4)	2.348(7)	Cd(1)-O(7)	2.297(8)
Cd(1)-O(1) ^{#1}	2.437(7)	Cd(1)-O(5)	2.318(7)	Cd(1)-N(3)	2.279(8)
Cd(1)-O(2)	2.451(8)				
Bond angles ($^\circ$)					
O(1)-Cd(1)-O(1) ^{#1}	72.9(3)	(1) ^{#1} -Cd(1)-O(4)	91.5(2)	O(2)-Cd(1)-N(3)	84.1(3)
O(1)-Cd(1)-O(2)	54.9(2)	(1) ^{#1} -Cd(1)-O(5)	81.8(2)	O(4)-Cd(1)-O(5)	56.6(3)
O(1)-Cd(1)-O(4)	93.9(3)	(1) ^{#1} -Cd(1)-O(7)	159.9(3)	O(4)-Cd(1)-O(7)	86.3(3)
O(1)-Cd(1)-O(5)	140.7(3)	(1) ^{#1} -Cd(1)-N(3)	81.2(3)	O(4)-Cd(1)-N(3)	156.2(3)
O(1)-Cd(1)-O(7)	127.2(3)	(2)-Cd(1)-O(4)	119.0(2)	(5)-Cd(1)-O(7)	80.3(3)
O(1)-Cd(1)-N(3)	105.3(3)	(2)-Cd(1)-O(5)	159.2(2)	(5)-Cd(1)-N(3)	99.8(3)
O(1) ^{#1} -Cd(1)-O(2)	118.9(2)	(2)-Cd(1)-O(7)	79.1(3)	(7)-Cd(1)-N(3)	92.8(3)
Intramolecular interactions (\AA)					
D-H...A	D-H (\AA)	H...A (\AA)	D...A (\AA)	>D-H...A ($^\circ$)	
C(23)-H(23)...O(4)	0.95	2.33	3.244(13)	160	
Intermolecular interactions (\AA)					
D-H...A	D-H (\AA)	H...A (\AA)	D...A (\AA)	>D-H...A ($^\circ$)	
O(7)-H(7A)...O(4)	0.67(16)	2.12(16)	2.729(13)	151(17)	
O(7)-H(7B)...O(3)	0.73(14)	2.03(15)	2.721(12)	158(16)	
N(1)-H(1N)...O(1W)	0.88	2.15	3.008(12)	165	
N(2)-H(2N)...O(2)	0.88	2.10	2.939(11)	158	
X-H...Cg(J)	H...Cg(J) (\AA)	H-Perp ^a (\AA)	γ ($^\circ$) ^b	X-H...Cg(J) ^c	X...Cg(J) (\AA)
C(1W)-H(1WB)...Cg(1)	2.95	2.70	24.18	143	3.788(16)
C(19)-H(19)...Cg(1)	2.69	2.67	6.71	147	3.525(12)
					54
					64

^a Perpendicular distance of H to ring plane J.

^b Angle between Cg(J)-H vector and ring J normal.

^c X-H...Cg(J) angle.

^d Angle of the X-H bond with the Pi-plane (Perpendicular = 90°, Parallel = 0°). #1: -x+1,-y+1,-z+1; Cg(1) = C(4) C(5) C(6) C(7) C(8) C(9).

tween 2.310(2)-2.4832(17) \AA and 54.59(6)-163.93(5) $^\circ$ (**2**), 2.258(4)-2.487(3) \AA and 53.84(11)-177.22(14) $^\circ$ (**3**), and 2.310(3)-2.520(3) \AA and 53.34(11)-174.00(16) $^\circ$ (**4**), showing similar values than other ladder-type Cd(II) CPs with the same linkers [41-44] (Table 3).

The different molecular arrangement of the studied CPs consisting on the presence of single (**1**) or double pillars (**2-4**) could be attributed to the difference in pKa values of the utilized N,N-donor spacers (pyz, 0.6 [45]; 4,4'-bipy, 3.17 [46]; 1,2-bpe, 3.89 [47]; 4,4'-azpy, 2.19 [48]). These values show that pyz presents the less coordinating ability and therefore, their competition with the coordina-

tion of water molecules should be higher than in the rest of linkers [49]. These results are in line with the observations regarding the obtention of **1**, since the trials to synthesize it using the same synthetic conditions as for the rest of compounds always promote the coordination of water molecules instead of pyz, leading to the $[\text{Cd}(\text{ACA})_2(\text{H}_2\text{O})_2]$ monomer.

The intramolecular interactions of **2-4** consist of $\pi\cdots\pi$ and C-H...O interactions. The torsion angles between the aromatic rings from the linkers evinced the higher planarity of 1,2-bpe (4.88 $^\circ$) and 4,4'-azpy (4.39 and 14.86 $^\circ$) in **3** and **4** compared with the 4,4'-bipy

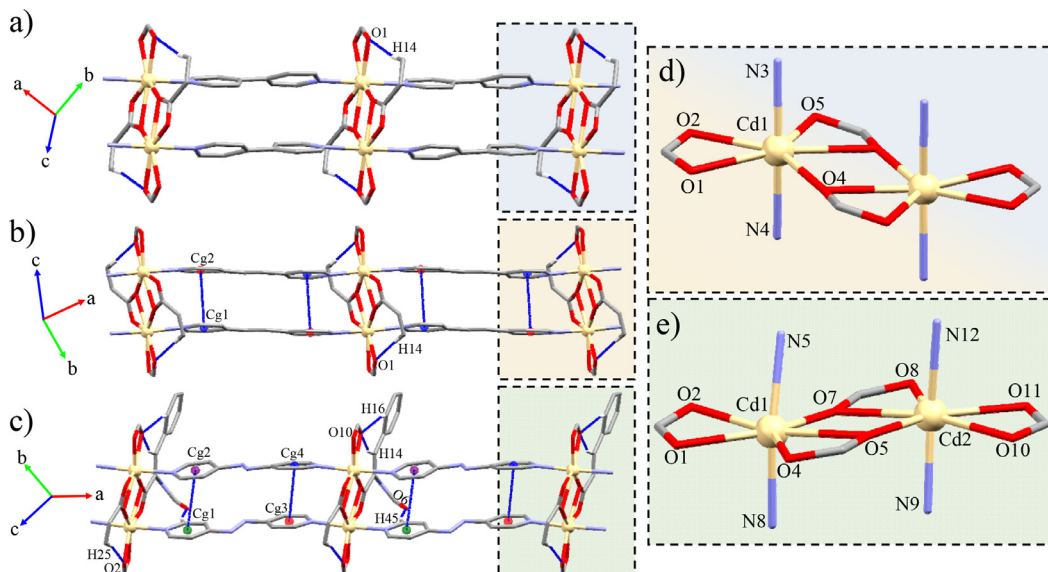


Fig. 2. Molecular structure of compounds (a) **2**, (b) **3**, and (c) **4**. In detail views of the SBUs in (d) **2** and **3**, and (e) **4**. All the atoms not involved in the highlighted interactions have been omitted for clarity.

Table 3
Selected bond lengths (\AA) and bond angles ($^\circ$) for **2-4**.

Bond lengths (\AA)					
Cd(1)-O(1)	2.3839(18)	Cd(1)-O(4)#2	2.3448(17)	Cd(1)-N(3)	2.310(2)
Cd(1)-O(2)	2.4012(19)	Cd(1)-O(5)	2.3874(16)	Cd(1)-N(4)#1	2.311(2)
Cd(1)-O(4)	2.4832(17)				
Bond angles ($^\circ$)					
O(1)-Cd(1)-O(2)	54.92(6)	O(2)-Cd(1)-O(4)#2	145.31(6)	O(4)-Cd(1)-N(4)#1	85.33(7)
O(1)-Cd(1)-O(4)	163.93(9)	O(2)-Cd(1)-O(5)	85.33(6)	O(4)#2-Cd(1)-O(5)	128.82(6)
O(1)-Cd(1)-O(4)#2	90.53(6)	O(2)-Cd(1)-N(3)	89.01(7)	O(4)#2-Cd(1)-N(3)	96.25(7)
O(1)-Cd(1)-O(5)	140.13(6)	O(2)-Cd(1)-N(4)#1	88.42(7)	O(4)#2-Cd(1)-N(4)#1	87.91(7)
O(1)-Cd(1)-N(3)	92.43(7)	O(4)-Cd(1)-O(4)#2	74.26(6)	O(5)-Cd(1)-N(3)	89.57(7)
O(1)-Cd(1)-N(4)#1	89.05(7)	O(4)-Cd(1)-O(5)	54.59(6)	O(5)-Cd(1)-N(4)#1	86.62(7)
O(2)-Cd(1)-O(4)	139.68(6)	O(4)-Cd(1)-N(3)	94.31(7)	N(3)-Cd(1)-N(4)#1	175.57(8)
Bond lengths (\AA)					
Cd(1)-O(1)	2.476(3)	Cd(1)-O(4)#2	2.487(3)	Cd(1)-N(3)	2.258(4)
Cd(1)-O(2)	2.320(3)	Cd(1)-O(5)#2	2.383(3)	Cd(1)-N(4)#1	2.267(4)
Cd(1)-O(4)	2.371(4)				
Bond angles ($^\circ$)					
O(1)-Cd(1)-O(2)	54.69(11)	O(2)-Cd(1)-O(4)#2	159.32(11)	O(4)-Cd(1)-N(4)#1	86.84(13)
O(1)-Cd(1)-O(4)	139.81(11)	O(2)-Cd(1)-O(5)#2	144.26(11)	O(4)#2-Cd(1)-O(5)#2	53.84(11)
O(1)-Cd(1)-O(4)#2	144.45(11)	O(2)-Cd(1)-N(3)	95.22(13)	O(4)#2-Cd(1)-N(3)	93.64(12)
O(1)-Cd(1)-O(5)#2	90.63(11)	O(2)-Cd(1)-N(4)#1	87.28(12)	O(4)#2-Cd(1)-N(4)#1	83.60(12)
O(1)-Cd(1)-N(3)	87.99(12)	O(4)-Cd(1)-O(4)#2	75.68(12)	O(5)#2-Cd(1)-N(3)	91.47(13)
O(1)-Cd(1)-N(4)#1	94.46(12)	O(4)-Cd(1)-O(5)#2	129.52(11)	O(5)#2-Cd(1)-N(4)#1	87.19(13)
O(2)-Cd(1)-O(4)	85.34(11)	O(4)-Cd(1)-N(3)	92.14(13)	N(3)-Cd(1)-N(4)#1	177.22(14)
Bond lengths (\AA)					
Cd(1)-O(1)	2.349(3)	Cd(1)-N(5)	2.318(3)	Cd(2)-O(10)	2.415(3)
Cd(1)-O(2)	2.370(3)	Cd(1)-N(8)#1	2.318(4)	Cd(2)-O(11)	2.345(3)
Cd(1)-O(4)	2.334(3)	Cd(2)-O(5)	2.339(3)	Cd(2)-N(9)	2.310(3)
Cd(1)-O(5)	2.520(3)	Cd(2)-O(7)	2.503(3)	Cd(2)-N(12)#2	2.317(4)
Cd(1)-O(7)	2.315(3)	Cd(2)-O(8)	2.373(3)		
Bond angles ($^\circ$)					
O(1)-Cd(1)-O(2)	55.86(11)	O(4)-Cd(1)-N(8)#1	93.35(12)	O(7)-Cd(2)-O(10)	165.63(11)
O(1)-Cd(1)-O(4)	81.30(12)	O(5)-Cd(1)-O(7)	77.39(10)	O(7)-Cd(2)-O(11)	135.96(11)
O(1)-Cd(1)-O(5)	134.95(11)	O(5)-Cd(1)-N(5)	82.66(11)	O(7)-Cd(2)-N(9)	83.36(12)
O(1)-Cd(1)-O(7)	147.65(11)	O(5)-Cd(1)-N(8)#1	96.67(12)	O(7)-Cd(2)-N(12)#2	100.80(12)
O(1)-Cd(1)-N(5)	99.70(13)	O(7)-Cd(1)-N(5)	83.17(14)	O(8)-Cd(2)-O(10)	138.62(12)
O(1)-Cd(1)-N(8)#1	88.20(12)	O(7)-Cd(1)-N(8)#1	86.48(12)	O(8)-Cd(2)-O(11)	83.37(12)
O(2)-Cd(1)-O(4)	136.51(12)	O(5)-Cd(1)-N(8)#1	169.52(16)	O(8)-Cd(2)-N(9)	92.64(14)
O(2)-Cd(1)-O(5)	165.89(10)	O(5)-Cd(2)-O(7)	77.31(10)	O(8)-Cd(2)-N(12)#2	93.32(13)
O(2)-Cd(1)-O(7)	92.51(12)	O(5)-Cd(2)-O(8)	129.96(11)	O(10)-Cd(2)-O(11)	55.30(12)
O(2)-Cd(1)-N(5)	86.40(11)	O(5)-Cd(2)-O(10)	91.42(12)	O(10)-Cd(2)-N(9)	87.61(12)
O(2)-Cd(1)-N(8)#1	92.47(12)	O(5)-Cd(2)-O(11)	146.59(11)	O(10)-Cd(2)-N(12)#2	87.45(13)
O(4)-Cd(1)-O(5)	53.77(11)	O(5)-Cd(2)-N(9)	89.00(15)	O(11)-Cd(2)-N(9)	92.01(14)
O(4)-Cd(1)-O(7)	130.85(11)	O(5)-Cd(2)-N(12)#2	87.71(13)	O(11)-Cd(2)-N(12)#2	87.98(13)
O(4)-Cd(1)-N(5)	94.63(13)	O(7)-Cd(2)-O(8)	53.34(11)	N(9)-Cd(2)-N(12)#2	174.00(16)

2. #1: $x-1, y+1, z$; #2: $-x, -y+2, -z$; **3.** #1: $x+1, y+1, z$; #2: $-x+1, -y+2, -z$; **4.** #1: $x-1, y, z$; #2: $x+1, y, z$.

Table 4
Selected intramolecular interactions (\AA) for **2-4**.

2	D-H···A	D-H (\AA)	H···A (\AA)	D···A (\AA)	>D-H···A ($^\circ$)
	C(14)-H(14)···O(1)	0.95	2.33	3.256(4)	166
3	D-H···A	D-H (\AA)	H···A (\AA)	D···A (\AA)	>D-H···A ($^\circ$)
	C(14)-H(14)···O(1)	0.95	2.20	3.139(6)	170
4	Cg(I)···Cg(J)	d_{Cg-Cg}^a (\AA)	α^b ($^\circ$)	β, γ^c ($^\circ$)	$d_{\text{plane-plane}}^d$ (\AA)
	Cg(1)···Cg(2)	3.744(4)	4.9(3)	27.5, 23.1	d_{offset}^e (\AA)
D-H···A					
4	D-H···A	D-H (\AA)	H···A (\AA)	D···A (\AA)	>D-H···A ($^\circ$)
	C(14)-H(14)···O(10)	0.95	2.40	3.311(6)	161
4	C(16)-H(16)···O(10)	0.95	2.51	3.381(7)	153
	C(25)-H(25)···O(2)	0.95	2.34	3.259(6)	163
4	C(45)-H(45)···O(6)	0.95	2.36	3.277(6)	163
	Cg(1)···Cg(J)	d_{Cg-Cg}^a (\AA)	α^b ($^\circ$)	β, γ^c ($^\circ$)	$d_{\text{plane-plane}}^d$ (\AA)
4	Cg(1)···Cg(2)	3.761(3)	3.2(3)	13.9, 17.2	0.907
	Cg(3)···Cg(4)	3.717(3)	8.7(3)	14.1, 19.7	0.904

^a Centroid-centroid distance. ^b Dihedral angle between the ring planes. ^c Offset angles: angle between Cg(I)-Cg(J) vector and normal to plane I, angle between Cg(I)-Cg(J) vector and normal to plane J ($\beta = \gamma$, when $\alpha = 0$). ^d Perpendicular distance of Cg(I) on plane J and perpendicular distance of Cg(J) on plane I (equal when $\alpha = 0$). ^e Horizontal displacement or slippage between Cg(I) and Cg(J) (equal for both centroids when $\alpha = 0$). **3:** Cg(1) = N(3) C(23) C(24) C(25) C(26) C(27); Cg(2) = N(4) C(30) C(31) C(32) C(33) C(34); **4:** Cg(1) = N(5) C(45) C(46) C(47) C(48) C(49); Cg(2) = N(12) C(60) C(61) C(62) C(63) C(64); Cg(3) = N(8) C(50) C(51) C(52) C(53) C(54); Cg(4) = N(9) C(55) C(56) C(57) C(58) C(59).

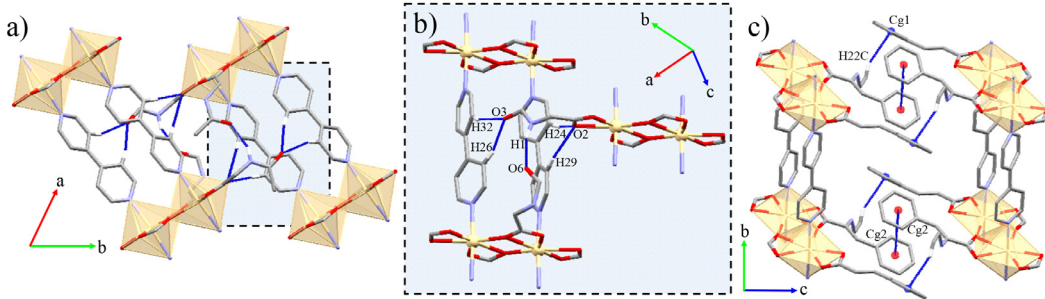
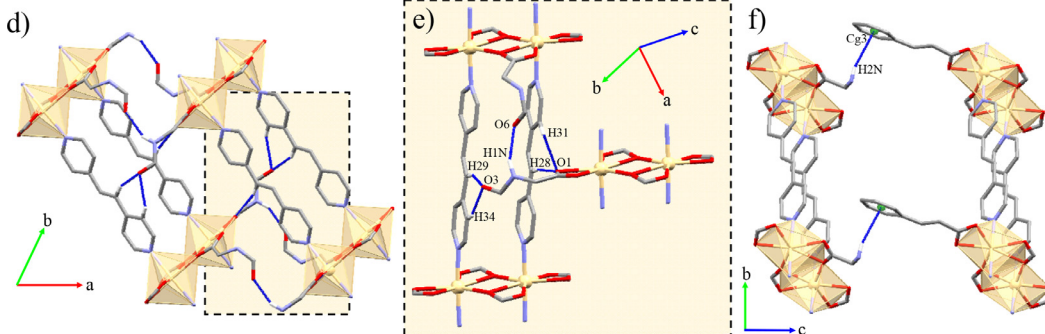
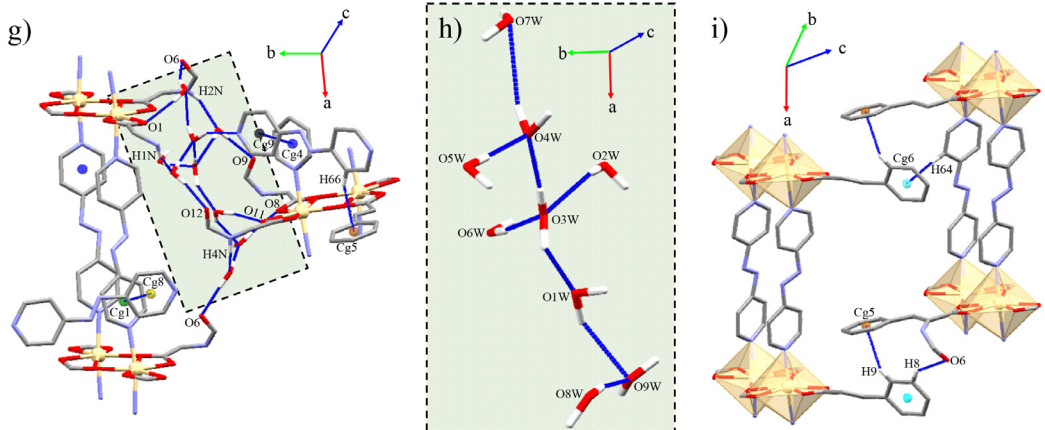
Compound 2**Compound 3****Compound 4**

Fig. 3. (a, d and g) General and (b, e and h) In detail views of the supramolecular interactions of **2-4** along the (110) plane. (c, f and i). General view of the supramolecular interactions of **2-4** along the (011) (**2** and **3**) and (101) (**4**) planes. All the atoms not involved in the highlighted interactions have been omitted for clarity.

of **2** (22.74°), allowing the stacking of their aromatic rings forming $\pi\cdots\pi$ interactions (Figs. 2a-c). In addition, compounds **2-4** display the same C-H···O interaction between the alkene H-atom of the $\mu_2\text{-}\eta^1:\eta^1$ ACA ligand and one of the oxygen atoms from a nearby $\mu_2\text{-}\eta^2$ ACA. Otherwise, in compound **4**, the torsion angles of the cinnamate skeletons of the $\mu_2\text{-}\eta^1:\eta^1$ ACA (8.47° and 12.27°) revealed their higher planarity in comparison with **2** and **3** (22.40° , **2**; 46.49° , **3**), permitting the C-H···O interaction between the o-H atom of this ACA and the oxygen atom from a $\mu_2\text{-}\eta^2$ ACA of the same dimeric SBU (Table 4).

3.5. Extended structure of complexes **2-4**

The supramolecular scaffold of **2** and **3** form 2D layers along the (110) plane (Fig. 3a and 3d), which are mainly held together by H-bonds involving the amide moieties from the $\mu_2\text{-}\eta^2$ ACA ligands, which joint together contiguous chains via amide-amide homosynthons. Moreover, there are additional C-H···O interactions in-

volving the carbonyl and carboxylate oxygen atoms from ACA with hydrogen atoms from nearby *N,N*-donor linkers (Fig. 3b and 3e). The presence of $\pi\cdots\pi$, C-H···π and N-H···π interactions extends the supramolecular scaffold along the [001] direction, forming the final 3D nets, presenting pccu topologies with different degrees of distortion, differently from the hxl topology of the 2D layers from **1**. (Table 5; Fig. 3c, 3f and 4).

In compound **4**, the azo group of 4,4'-azpy promotes a change in its crystal packing compared with **2** and **3**, allowing the introduction of one non-coordinated 4,4'-azpy and nine water molecules into the supramolecular network (Figs. 3 and 5). This effect has been previously observed by Kitagawa et al. [50], and is attributed to the electronic repulsions between the lone pair electrons of the carboxylate oxygen atoms and the azo groups. Therefore, the non-coordinated water molecules drive the supramolecular assembly connecting the polymeric chains via H-bonding with the NH and C=O moieties from contiguous amide groups and the carboxylate groups from ACA ligands of nearby chains, extending

Table 5
Selected intermolecular interactions (\AA) for **2-4**.

2	D-H...A	D-H (\AA)	H...A (\AA)	D...A (\AA)	>D-H...A ($^{\circ}$)		
	N(1)-H(1)...O(6)	0.88	1.99	2.811(3)	155		
	C(24)-H(24)...O(2)	0.95	2.41	3.321(4)	161		
	C(26)-H(26)...O(3)	0.95	2.41	3.329(5)	162		
	C(29)-H(29)...O(2)	0.95	2.62	3.554(4)	167		
	C(32)-H(32)...O(3)	0.95	2.10	2.958(4)	149		
	X-H...Cg(J)	H...Cg(J) (\AA)	H-Perp ^a (\AA)	γ ($^{\circ}$) ^b	X-H...Cg(J) ^c ($^{\circ}$)	X...Cg(J) (\AA)	X-H, Pi ^d ($^{\circ}$)
	C(22)-H(22C)...Cg(1)	2.69	2.67	7.71	159	3.623(4)	74
	Cg(I)...Cg(J)	d _{Cg-Cg} ^e (\AA)	α ^f ($^{\circ}$)	β , γ ^g ($^{\circ}$)	d _{plane-plane} ^h (\AA)	d _{offset} ⁱ (\AA)	
	Cg(2)...Cg(2)	3.861(2)	0	28.3, 28.3	3.3980(14)	1.833	
3	D-H...A	D-H (\AA)	H...A (\AA)	D...A (\AA)	>D-H...A ($^{\circ}$)		
	N(1)-H(1N)...O(6)	0.88	2.07	2.889(6)	154		
	C(28)-H(28)...O(1)	0.95	2.35	3.277(6)	165		
	C(29)-H(29)...O(3)	0.95	2.43	3.321(7)	156		
	C(31)-H(31)...O(1)	0.95	2.62	3.553(7)	167		
	C(34)-H(34)...O(3)	0.95	2.52	3.384(7)	151		
	X-H...Cg(J)	H...Cg(J) (\AA)	H-Perp ^a (\AA)	γ ($^{\circ}$) ^b	X-H...Cg(J) ^c ($^{\circ}$)	X...Cg(J) (\AA)	X-H, Pi ^d ($^{\circ}$)
	N(2)-H(2N)...Cg(3)	2.72	2.61	16.71	163	3.573(5)	68
4	D-H...A	D-H (\AA)	H...A (\AA)	D...A (\AA)	>D-H...A ($^{\circ}$)		
	O(1W)-H(1WA)...O(11)	0.96(7)	1.84(7)	2.792(5)	170(7)		
	N(1)-H(1N)...O(5W)	0.88	1.99	2.823(6)	159		
	O(1W)-H(1WB)...O(9W)	0.99(5)	2.03(6)	2.856(5)	139(6)		
	N(2)-H(2N)...O(2W)	0.88	1.98	2.785(6)	151		
	N(3)-H(3)...O(3)	0.88	2.12	2.856(6)	141		
	O(2W)-H(2WA)...O(9)	0.77(8)	1.96(8)	2.723(6)	171(8)		
	O(2W)-H(2WB)...O(3W)	0.79(8)	2.05(8)	2.768(7)	150(7)		
	N(4)-H(4N)...O(8W)	0.88	2.18	2.998(6)	154		
	O(3W)-H(3WA)...O(4W)	0.85(8)	1.87(8)	2.715(6)	175(10)		
	O(3W)-H(3WB)...O(1W)	0.97(9)	1.81(8)	2.704(7)	152(6)		
	O(4W)-H(4WA)...O(7W)	0.78(9)	2.43(8)	3.107(9)	147(7)		
	O(4W)-H(4WB)...N(16)	0.88(7)	1.98(7)	2.776(6)	150(7)		
	O(5W)-H(5WA)...O(12)	0.85(7)	1.88(7)	2.718(6)	171(7)		
	O(5W)-H(5WB)...O(4W)	0.83(7)	2.02(7)	2.853(6)	177(8)		
	O(6W)-H(6WB)...O(3W)	0.82(8)	1.97(7)	2.780(8)	170(13)		
	O(7W)-H(7WA)...O(1)	0.83(7)	2.01(7)	2.831(7)	173(6)		
	O(7W)-H(7WB)...O(6)	0.83(8)	2.32(7)	3.084(7)	153(7)		
	O(8W)-H(8WA)...O(6)	0.91(8)	2.00(8)	2.903(6)	172(7)		
	O(8W)-H(8WB)...O(9W)	0.88(7)	2.17(7)	3.042(6)	169(6)		
	O(9W)-H(9WA)...O(8)	0.88(7)	1.86(8)	2.726(6)	167(6)		
	O(9W)-H(9WB)...O(3)	0.84(7)	2.20(6)	2.954(5)	149(7)		
	C(8)-H(8)...O(6)	0.95	2.52	3.331(7)	143		
	C(18)-H(18)...O(5W)	0.95	2.38	3.185(7)	142		
	C(33)-H(33A)...O(3)	0.98	2.43	3.228(8)	138		
	X-H...Cg(J)	H...Cg(J) (\AA)	H-Perp ^a (\AA)	γ ($^{\circ}$) ^b	X-H...Cg(J) ^c ($^{\circ}$)	X...Cg(J) (\AA)	X-H, Pi ^d ($^{\circ}$)
	C(9)-H(9)...Cg(5)	2.74	2.70	9.53	152	3.606(7)	61
	C(64)-H(64)...Cg(6)	2.71	2.64	13.36	152	3.574(7)	56
	C(66)-H(66)...Cg(5)	2.63	2.62	4.61	150	3.483(8)	60
	C(74)-H(74)...Cg(7)	2.92	2.77	18.49	134	3.645(8)	59
	Cg(I)...Cg(J)	d _{Cg-Cg} ^e (\AA)	α ^f ($^{\circ}$)	β , γ ^g ($^{\circ}$)	d _{plane-plane} ^h (\AA)	d _{offset} ⁱ (\AA)	
	Cg(1)...Cg(8)	3.848(3)	22.4(2)	8.5, 26.4	3.4444(19), 3.805(2)	0.569	
	Cg(4)...Cg(9)	3.935(4)	10.7(3)	18.9, 25.5	3.553(2), 3.724(3)	1.273	

^a Perpendicular distance of H to ring plane J. ^b Angle between Cg(J)-H vector and ring J normal. ^c X-H...Cg(J) angle. ^d Angle of the X-H bond with the Pi-plane (Perpendicular = 90°, Parallel = 0°). ^e Centroid-centroid distance. ^f Dihedral angle between the ring planes. ^g Offset angles: angle between Cg(I)-Cg(J) vector and normal to plane I, angle between Cg(I)-Cg(J) vector and normal to plane J ($\beta = \gamma$, when $\alpha = 0$). ^h Perpendicular distance of Cg(I) on plane J and perpendicular distance of Cg(J) on plane I (equal when $\alpha = 0$). ⁱ Horizontal displacement or slippage between Cg(I) and Cg(J) (equal for both centroids when $\alpha = 0$). **2:** Cg(1) = C(4) C(5) C(6) C(7) C(8) C(9); Cg(2) = C(15) C(16) C(17) C(18) C(19) C(20). **3:** Cg(3) = C(4) C(5) C(6) C(7) C(8) C(9). **4:** Cg(1) = N(5) C(45) C(46) C(47) C(48) C(49); Cg(4) = N(9) C(55) C(56) C(57) C(58) C(59); Cg(5) = C(15) C(16) C(17) C(18) C(19) C(20); Cg(6) = C(4) C(5) C(6) C(7) C(8) C(9); Cg(7) = C(26) C(27) C(28) C(29) C(30) C(31); Cg(8) = N(13) C(65) C(66) C(67) C(68) C(69); Cg(9) = N(16) C(70) C(71) C(72) C(73) C(74).

the structure through the (110) plane (Fig. 3g). In addition, the water molecules form supramolecular patterns of H-bonds between them (Fig. 3h). The non-coordinated 4,4'-azpy molecules also contribute to the formation of this plane through their $\pi\cdots\pi$ stacking with the pillarating 4,4'-azpy linkers (Fig. 5c). Finally, additional C-H...O and C-H... π interactions extend the structure forming the final 3D network (Table 5, Fig. 3i).

3.6. Photophysical properties

The solid-state UV-Vis and fluorescence measurements of complexes **1-4** have been recorded. Their absorption spectra show

overlapped bands centered at 252 and 302 nm (**1**), 264 and 293 nm (**2**), 276 and 329 nm (**3**), and 284 and 345 nm (**4**) (SI: Fig. S18). Moreover, compound **4** presents an additional absorption band centered at 470 nm. The comparison of these results with the corresponding free ligands shows that the common peaks of **1-4** should be mainly attributed to a combination of absorptions of the $\pi\cdots\pi^*$ transitions of the former ligands of each CP, where a higher contribution of the ACA ligand (λ_{\max} (HACA) = 246 nm, 294 nm) should be associated to the first band, and the second band might be more dependent of the N,N-donor linkers [51–54]. In addition, the band centered at 470 nm in **4** has been attributed to the n- π^* transitions of the 4,4'-azpy ligand, mainly centered in the azo chromophore [55].

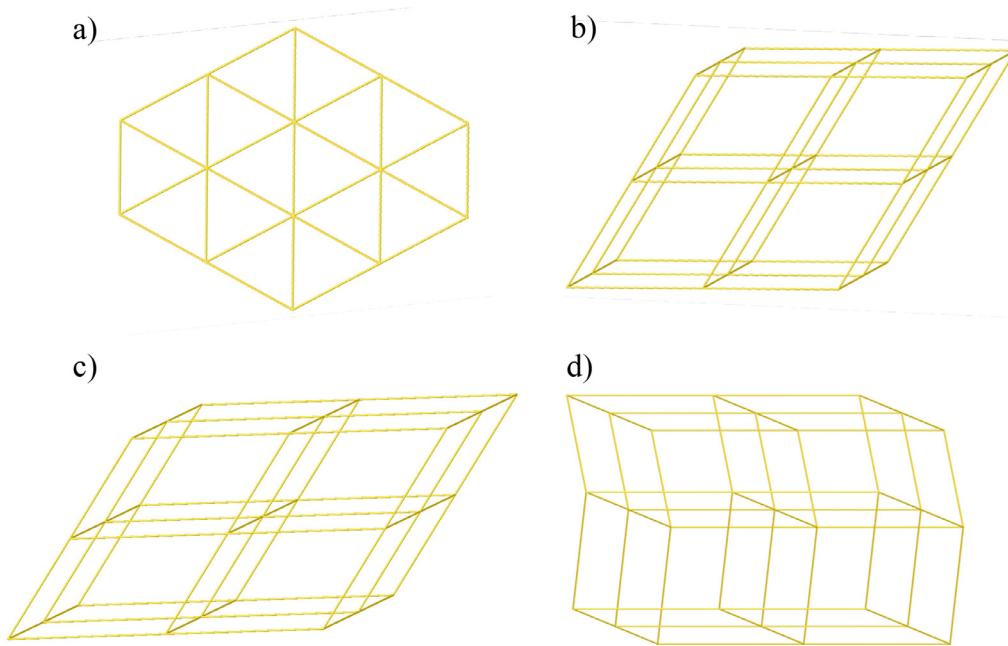


Fig. 4. Topological analysis of (a) compound **1** displaying a 2D layer with hxl topology. (b-d) Compounds **2-4** forming 3D networks with pcu topologies.

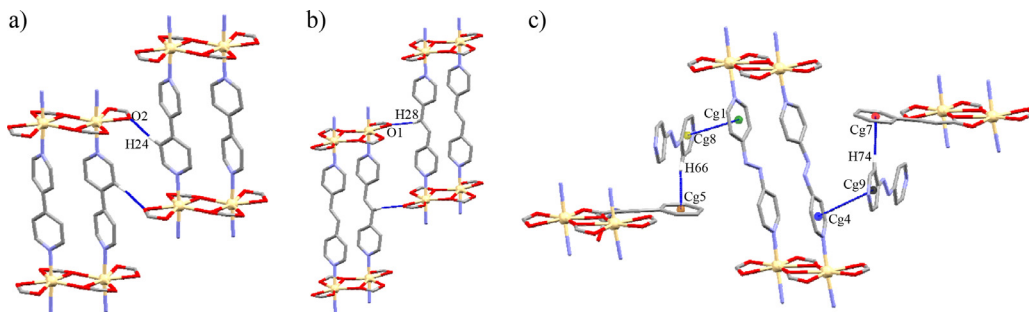


Fig. 5. Disposition of the chains in: (a) **2**, (b) **3**, and (c) **4**, showing the effect of the azo group in **4**, which drives a different supramolecular packing compared with **2** and **3**. All the atoms not involved in the highlighted interactions have been omitted for clarity.

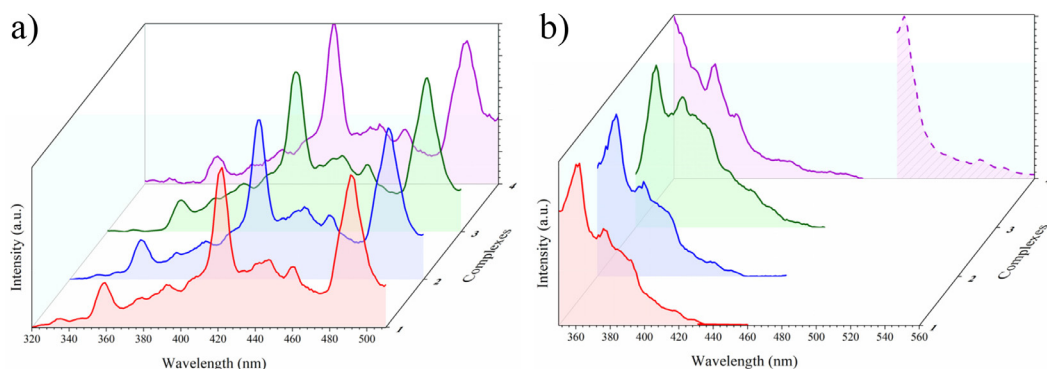


Fig. 6. Normalized solid-state emission spectra of compounds **1-4** excited at: (a) 262 nm showing emission peaks around 359, 422 and 491 nm. (b) 315 nm showing emission peaks around 360, 376 and 392 nm. The dashed line of capture (b) corresponds to the emission of **4** when excited at 470 nm, showing an emission peak at 484 nm.

When all the compounds were irradiated at their first absorption band ($\lambda_{\text{exc}} = 262 \text{ nm}$), all of them display the same pattern of unstructured emission signals with different maxima in the range of 320–500 nm, and moderate Stokes shift between 10235 and 17884 cm^{-1} (Fig. 6a). Relevant emission maxima and Stokes shifts are listed in the SI (Table S2). Besides, the irradiation of the complexes at their second absorption band ($\lambda_{\text{exc}} = 315 \text{ nm}$) show the emission of similar unstructured bands but with a lower range, probably due to the use of a less energetic ir-

radiation (Fig. 6b). Finally, when compound **4** was irradiated at 470 nm, the emission of the azo chromophore has been observed, displaying a peak at 484 nm (Fig. 6b). Considering these excitations, the resulting emission colors according to the CIE 1931 chromaticity diagrams when irradiated at 262 nm are blue ribbon (**1-3**) and azure radiance (**4**), while when $\lambda_{\text{exc}} = 315 \text{ nm}$ the observed color was electric violet (**1-4**), and the excitation of the azo chromophore of **4** at 470 nm results in a cyan color (SI: Fig. S19).

4. Conclusions

We have successfully synthesized four Cd(II) CPs, whose structural elucidation revealed the formation of 1D ladder-type arrangements with single (**1**) and double (**2–4**) pillars depending on the *N,N*-donor spacer coordination ability (pyz<4,4'-azpy<4,4'-bipy<1,2-bpe). Interestingly, the incorporation of an azo group in the spacer of **4**, resulted in a different crystal packing owing to the repulsion between the N=N group and the oxygen atoms from the carboxylate ACA ligands, leading to the introduction of one non-coordinated 4,4'-azpy and nine water molecules in their supramolecular structure. The CPs **2–4** have been synthesized using Milli-Q water, while **1** has been prepared in EtOH owing to the competition between the pyz and water molecules, which lead to $[Cd(ACA)_2(H_2O)_2]$ when the reaction was performed in Milli-Q water. In addition, the solid-state photophysical properties show the combined emission of the ACA and the corresponding *N,N*-donor linkers displaying emissions in the blue range, showing different tonalities from violet to cyan. Therefore, this work contributes to the understanding of the influence of little modifications of *N,N*-donor based spacers on the structure and photophysical properties of Cd(II) CPs.

Declaration of Competing Interest

The authors declare that they have no known competing financial interests or personal relationships that could have appeared to influence the work reported in this paper.

CRediT authorship contribution statement

Daniel Ejarque: Methodology, Software, Formal analysis, Investigation, Data curation, Writing – original draft, Visualization. **Teresa Calvet:** Validation, Resources. **Mercè Font-Bardia:** Formal analysis, Data curation. **Josefina Pons:** Conceptualization, Validation, Resources, Writing – review & editing, Supervision, Project administration, Funding acquisition.

Data availability

Data will be made available on request.

Acknowledgements

J.P. acknowledges financial support from the CB615921 project, the CB616406 project from “Fundació La Caixa,” and the 2017SGR1687 project from the Generalitat de Catalunya. D.E. acknowledges the PIF predoctoral fellowship from the Universitat Autònoma de Barcelona.

Supplementary materials

Supplementary material associated with this article can be found, in the online version, at doi:[10.1016/j.molstruc.2022.134896](https://doi.org/10.1016/j.molstruc.2022.134896).

References

- [1] C.B. Aakeröy, N.R. Champness, C. Janiak, Recent advances in crystal engineering, *CrystEngComm* 12 (2010) 22–43, doi:[10.1039/B919819A](https://doi.org/10.1039/B919819A).
- [2] M. Du, C.-P. Li, C.-S. Liu, S.-M. Fang, Design and construction of coordination polymers with mixed-ligand synthetic strategy, *Coord. Chem. Rev.* 257 (2013) 1282–1305, doi:[10.1016/j.ccr.2012.10.002](https://doi.org/10.1016/j.ccr.2012.10.002).
- [3] W.P. Lustig, S. Mukherjee, N.D. Rudd, A.V. Desai, J. Li, S.K. Ghosh, Metal–organic frameworks: functional luminescent and photonic materials for sensing applications, *Chem. Soc. Rev.* 46 (2017) 3242–3285, doi:[10.1039/C6CS00930A](https://doi.org/10.1039/C6CS00930A).
- [4] W.-Q. Kan, S.-Z. Wen, A fluorescent coordination polymer for selective sensing of hazardous nitrobenzene and dichromate anion, *Dyes Pigments* 139 (2017) 372–380, doi:[10.1016/j.dyepig.2016.12.039](https://doi.org/10.1016/j.dyepig.2016.12.039).
- [5] S.-D. Han, J.-X. Hu, G.-M. Wang, Recent advances in crystalline hybrid photochromic materials driven by electron transfer, *Coord. Chem. Rev.* 452 (2022) 214304, doi:[10.1016/j.ccr.2021.214304](https://doi.org/10.1016/j.ccr.2021.214304).
- [6] Q. Yue, E.-Q. Gao, Azide and carboxylate as simultaneous coupler for magnetic coordination polymers, *Coord. Chem. Rev.* 382 (2019) 1–31, doi:[10.1016/j.ccr.2018.12.002](https://doi.org/10.1016/j.ccr.2018.12.002).
- [7] S.-D. Han, J.-X. Hu, J.-H. Li, G.-M. Wang, Anchoring polydentate N/O-ligands in metal phosphite/phosphate/phosphonate (MPO) for functional hybrid materials, *Coord. Chem. Rev.* 475 (2023) 214892, doi:[10.1016/j.ccr.2022.214892](https://doi.org/10.1016/j.ccr.2022.214892).
- [8] Y. Chen, M. Tang, Y. Wu, X. Su, X. Li, S. Xu, S. Zhuo, J. Ma, D. Yuan, C. Wang, W. Hu, A one-dimensional π -d conjugated coordination polymer for sodium storage with catalytic activity in Negishi coupling, *Angew. Chem. Int. Ed.* 58 (2019) 14731–14739, doi:[10.1002/anie.201908274](https://doi.org/10.1002/anie.201908274).
- [9] A. Angulo-Ibáñez, G. Beobide, O. Castillo, A. Luque, S. Pérez-Yáñez, D. Vallejo-Sánchez, Aerogels of 1D coordination polymers: from a non-porous metal-organic crystal structure to a highly porous material, *Polymers* 8 (2016) 16, doi:[10.3390/polym8010016](https://doi.org/10.3390/polym8010016).
- [10] A. Worthy, A. Grosjean, M.C. Pfrunder, Y. Xu, C. Yan, G. Edwards, J.K. Clegg, J.C. McMurtrie, Atomic resolution of structural changes in elastic crystals of copper(II) acetylacetone, *Nat. Chem.* 10 (2018) 65–69, doi:[10.1038/nchem.2848](https://doi.org/10.1038/nchem.2848).
- [11] A. Barbieri, G. Accorsi, N. Armaroli, Luminescent complexes beyond the platinum group: the d¹⁰ avenue, *Chem. Commun.* (2008) 2185–2193, doi:[10.1039/b716650h](https://doi.org/10.1039/b716650h).
- [12] Y. Mu, Y. Ran, B. Zhang, J. Du, C. Jiang, J. Du, Dicarboxylate ligands modulated structural diversity in the construction of Cd(II) coordination polymers built from N-heterocyclic ligand: synthesis, structures, and luminescent sensing, *Cryst. Growth Des.* 20 (2020) 6030–6043, doi:[10.1021/acs.cgd.0c00739](https://doi.org/10.1021/acs.cgd.0c00739).
- [13] M. Borsari, Cadmium: coordination chemistry, in: R.A. Scott (Ed.), *Encycl. Inorg. Bioinorg. Chem.*, 2nd ed., John Wiley & Sons, Ltd, Chichester, UK, 2014, pp. 1–16, doi:[10.1002/9781119951438.eibc2261](https://doi.org/10.1002/9781119951438.eibc2261).
- [14] R.D. Shannon, Revised effective ionic radii and systematic studies of interatomic distances in halides and chalcogenides, *Acta Cryst. A* 32 (1976) 751–767, doi:[10.1107/S0567739476001551](https://doi.org/10.1107/S0567739476001551).
- [15] A.L. Allred, Electronegativity values from thermochemical data, *J. Inorg. Nucl. Chem.* 17 (1961) 215–221, doi:[10.1016/0022-1902\(61\)80142-5](https://doi.org/10.1016/0022-1902(61)80142-5).
- [16] R.D. Hancock, The pyridyl group in ligand design for selective metal ion complexation and sensing, *Chem. Soc. Rev.* 42 (2013) 1500–1524, doi:[10.1039/C2CS35224A](https://doi.org/10.1039/C2CS35224A).
- [17] Y. Wang, H. Cao, B. Zheng, R. Zhou, J. Duan, Solvent- and pH-dependent formation of four zinc porous coordination polymers: framework isomerism and gas separation, *Cryst. Growth Des.* 18 (2018) 7674–7682, doi:[10.1021/acs.cgd.8b01433](https://doi.org/10.1021/acs.cgd.8b01433).
- [18] C.A. Hollis, S.R. Batten, C.J. Sumby, Two-dimensional and three-dimensional coordination polymers of hexakis(4-cyanophenyl)[3]radialene: the role of stoichiometry and kinetics, *Cryst. Growth Des.* 13 (2013) 2350–2361, doi:[10.1021/cg400036x](https://doi.org/10.1021/cg400036x).
- [19] Y.-Y. Jia, G.-J. Ren, A.-L. Li, L.-Z. Zhang, R. Feng, Y.-H. Zhang, X.-H. Bu, Temperature-related synthesis of two anionic metal–organic frameworks with distinct performance in organic dye adsorption, *Cryst. Growth Des.* 16 (2016) 5593–5597, doi:[10.1021/acs.cgd.6b00813](https://doi.org/10.1021/acs.cgd.6b00813).
- [20] X.-Q. Liang, D.-P. Li, X.-H. Zhou, Y. Sui, Y.-Z. Li, J.-L. Zuo, X.-Z. You, Metal–organic coordination polymers generated from chiral camphoric acid and flexible ligands with different spacer lengths: syntheses, structures, and properties, *Cryst. Growth Des.* 9 (2009) 4872–4883, doi:[10.1021/cg900676x](https://doi.org/10.1021/cg900676x).
- [21] C. Jiao, J. Geng, C. He, G. Cui, Assembly multi-dimensional Cd^{II} coordination architectures based on flexible bis(benzimidazole) ligands: diversity of their coordination geometries and fluorescent properties, *J. Mol. Struct.* 1020 (2012) 134–141, doi:[10.1016/j.jmolstruc.2012.03.051](https://doi.org/10.1016/j.jmolstruc.2012.03.051).
- [22] S. Kamal, A.I. Inamdar, K. Chiou, B. Sainbileg, M. Usman, J. Chen, T. Luo, M. Hayashi, C. Hung, W. Liaw, K. Lu, Functional groups assisted tunable dielectric permittivity of guest-free Zn-based coordination polymers for gate dielectrics, *Chem. Eur. J.* 28 (2022) e2021039, doi:[10.1002/chem.202103905](https://doi.org/10.1002/chem.202103905).
- [23] M. Dai, L.-W. Zhu, J.-H. Yang, H.-X. Li, M.-M. Chen, Z.-G. Ren, J.-P. Lang, Spacer length effect on the formation of different zinc coordination polymers of 1,4-benzenedicarboxylate and flexible bipyrazolyl ligands, *Inorg. Chem. Commun.* 29 (2013) 70–75, doi:[10.1016/j.jinoche.2012.11.038](https://doi.org/10.1016/j.jinoche.2012.11.038).
- [24] H. Doan, F. Cheng, T. Dyirakumunda, M. Elsegood, J. Chin, O. Rowe, C. Redshaw, V. Ting, Using supercritical CO₂ in the preparation of metal–organic frameworks: investigating effects on crystallisation, *Crystals* 10 (2019) 17, doi:[10.3390/cryst10010017](https://doi.org/10.3390/cryst10010017).
- [25] D. Ejarque, F. Sánchez-Férez, T. Calvet, M. Font-Bardia, J. Pons, Exploring the reactivity of α -acetamidocinnamic acid and 4-phenylpyridine with Zn(II) and Cd(II), *Inorg. Chim. Acta* 509 (2020) 119695, doi:[10.1016/j.ica.2020.119695](https://doi.org/10.1016/j.ica.2020.119695).
- [26] D. Ejarque, T. Calvet, M. Font-Bardia, J. Pons, Construction of Zn(II) linear trinuclear secondary building units from a coordination polymer based on α -acetamidocinnamic acid and 4-phenylpyridine, *Molecules* 25 (2020) 3615, doi:[10.3390/molecules25163615](https://doi.org/10.3390/molecules25163615).
- [27] D. Ejarque, T. Calvet, M. Font-Bardia, J. Pons, Steric crowding of a series of pyridine based ligands influencing the photophysical properties of Zn(II) complexes, *CrystEngComm* 23 (2021) 6199–6213, doi:[10.1039/d1ce00833a](https://doi.org/10.1039/d1ce00833a).
- [28] D. Ejarque, T. Calvet, M. Font-Bardia, J. Pons, Influence of a series of pyridine ligands on the structure and photophysical properties of Cd(II) complexes, *CrystEngComm* 24 (2022) 2808–2824, doi:[10.1039/d1ce01584b](https://doi.org/10.1039/d1ce01584b).

- [29] D. Ejarque, T. Calvet, M. Font-Bardia, J. Pons, Amide-driven secondary building unit structural transformations between Zn(II) coordination polymers, *Cryst. Growth Des.* 22 (2022) 5012–5026, doi:[10.1021/acs.cgd.2c00520](https://doi.org/10.1021/acs.cgd.2c00520).
- [30] G.M. Sheldrick, A short history of SHELX, *Acta Cryst. A* 64 (2008) 112–122, doi:[10.1107/S0108767307043930](https://doi.org/10.1107/S0108767307043930).
- [31] C.F. MacRae, I. Sovago, S.J. Cottrell, P.T.A. Galek, P. McCabe, E. Pidcock, M. Platings, G.P. Shields, J.S. Stevens, M. Towler, P.A. Wood, Mercury 4.0: from visualization to analysis, design and prediction, *J. Appl. Cryst.* 53 (2020) 226–235, doi:[10.1107/S1600576719014092](https://doi.org/10.1107/S1600576719014092).
- [32] Persistence of Vision Pty. Ltd Persistence of Vision (TM) Raytracer, Persistence of Vision Pty. Ltd, Williamstown, Australia, 2004.
- [33] O.V. Dolomanov, L.J. Bourhis, R.J. Gildea, J.A.K. Howard, H. Puschmann, OLEX2 : a complete structure solution, refinement and analysis program, *J. Appl. Cryst.* 42 (2009) 339–341, doi:[10.1107/S0021889808042726](https://doi.org/10.1107/S0021889808042726).
- [34] A.L. Spek, Single-crystal structure validation with the program PLATON, *J. Appl. Cryst.* 36 (2003) 7–13, doi:[10.1107/S0021889802022112](https://doi.org/10.1107/S0021889802022112).
- [35] M. Llunell, D. Casanova, J. Cirera, P. Alemany, S. Alvarez, SHAPE. Program for the Stereochemical Analysis of Molecular Fragments by Means of Continuous Shape Measures and Associated Tools, Universitat de Barcelona, Barcelona, 2013.
- [36] G.B. Deacon, R.J. Phillips, Relationships between the carbon-oxygen stretching frequencies of carboxylato complexes and the type of carboxylate coordination, *Coord. Chem. Rev.* 33 (1980) 227–250, doi:[10.1016/S0010-8545\(00\)80455-5](https://doi.org/10.1016/S0010-8545(00)80455-5).
- [37] K. Nakamoto, Infrared and Raman Spectra of Inorganic and Coordination Compounds: Part A: Theory and Applications in Inorganic Chemistry, 6th ed., Wiley Interscience, Hoboken, New Jersey, USA, 2009, doi:[10.1002/9780470405840](https://doi.org/10.1002/9780470405840).
- [38] D.H. Williams, I. Fleming, Spectroscopic Methods in Organic Chemistry, 7th ed., Springer Nature, Cham, Switzerland, 2008, doi:[10.1002/star.19860380313](https://doi.org/10.1002/star.19860380313).
- [39] H. Mao, C. Zhang, G. Li, H. Zhang, H. Hou, L. Li, Q. Wu, Y. Zhu, E. Wang, New types of the flexible self-assembled metal-organic coordination polymers constructed by aliphatic dicarboxylates and rigid bidentate nitrogen ligands, *Dalton Trans.* (2004) 3918–3925, doi:[10.1039/B410235E](https://doi.org/10.1039/B410235E).
- [40] D. Chisca, A.V. Siminel, M.S. Fonari, L. Croitor, Structural characterization and emission properties of mixed-ligand transition metal coordination complexes with dicarboxylic acids and pyrazinecarboxamide, *Polyhedron* 170 (2019) 245–252, doi:[10.1016/j.poly.2019.05.052](https://doi.org/10.1016/j.poly.2019.05.052).
- [41] H.-L. Jiang, Y. Tatsu, Z.-H. Lu, Q. Xu, Non-, micro-, and mesoporous metal-organic framework isomers: reversible transformation, fluorescence sensing, and large molecule separation, *J. Am. Chem. Soc.* 132 (2010) 5586–5587, doi:[10.1021/ja101541s](https://doi.org/10.1021/ja101541s).
- [42] D. Liu, N.-Y. Li, J.-P. Lang, Single-crystal to single-crystal transformation of 1D coordination polymervia photochemical [2+2] cycloaddition reaction, *Dalton Trans.* 40 (2011) 2170–2172, doi:[10.1039/C0DT00931H](https://doi.org/10.1039/C0DT00931H).
- [43] F. Kettner, C. Worch, J. Moellmer, R. Gläser, R. Staudt, H. Krautscheid, Synthesis, crystal structure and catalytic behavior of homo- and heteronuclear coordination polymers [M(tdc)(bpy)] ($M^{2+} = Fe^{2+}, Co^{2+}, Zn^{2+}, Cd^{2+}$; tdc $^{2-}$ = 2,5-thiophenedicarboxylate), *Inorg. Chem.* 52 (2013) 8738–8742, doi:[10.1021/ic400857s](https://doi.org/10.1021/ic400857s).
- [44] A. Półrolnickzak, A. Katrusiak, Self-healing ferroelastic metal-organic framework sensing guests, pressure and chemical environment, *Mater. Adv.* 2 (2021) 4677–4684, doi:[10.1039/D1MA00111F](https://doi.org/10.1039/D1MA00111F).
- [45] A.S. Chía, R.F. Trimble Jr., Acid-base properties of some pyrazines, *J. Chem. Phys.* 65 (1961) 863–866.
- [46] J. Sendh, M.P. Singh, J.B. Baruah, 5-[Pyren-9-ylmethyl]aminoisophthalic acid with nitrogen containing heterocycles: stacking, N-H···π interactions and photoluminescence, *CrystEngComm* 23 (2021) 6952–6966, doi:[10.1039/DCE01099A](https://doi.org/10.1039/DCE01099A).
- [47] V. Kumar, P.K. Goswami, S.Tewari Balendra, A. Ramanan, Multicomponent solids of niflumic and mefenamic acids based on acid-pyridine synthon, *Front. Chem.* 10 (2022) 729608, doi:[10.3389/fchem.2022.729608](https://doi.org/10.3389/fchem.2022.729608).
- [48] P. Ravat, S. Seethalekshmi, S.N. Biswas, P. Nandy, S. Varughese, Equivalence of ethylene and azo-bridges in the modular design of molecular complexes: role of weak interactions, *Cryst. Growth Des.* 15 (2015) 2389–2401, doi:[10.1021/acs.cgd.5b00183](https://doi.org/10.1021/acs.cgd.5b00183).
- [49] E.G. Percástegui, T.K. Ronson, J.R. Nitschke, Design and applications of water-soluble coordination cages, *Chem. Rev.* 120 (2020) 13480–13544, doi:[10.1021/cr000672](https://doi.org/10.1021/cr000672).
- [50] T.K. Maji, K. Uemura, H.-C. Chang, R. Matsuda, S. Kitagawa, Expanding and shrinking porous modulation based on pillared-layer coordination polymers showing selective guest adsorption, *Angew. Chem.* 116 (2004) 3331–3334, doi:[10.1002/ange.200453923](https://doi.org/10.1002/ange.200453923).
- [51] S. Xu, Y. Wu, B. Chen, P. Huang, Z. Zhang, Y. Zhong, Y. Zhao, X. Huang, K. Du, Electrochemical thin film deposition of copper(I) halides in aqueous solution: substrate extension and structure transformation, *Adv. Mater. Interfaces* 9 (2022) 2102239, doi:[10.1002/admi.202102239](https://doi.org/10.1002/admi.202102239).
- [52] J.-J. Wang, C.-S. Liu, T.-L. Hu, Z. Chang, C.-Y. Li, L.-F. Yan, P.-Q. Chen, X.-H. Bu, Q. Wu, L.-J. Zhao, Z. Wang, X.-Z. Zhang, Zinc(II) coordination architectures with two bulky anthracene-based carboxylic ligands: crystal structures and luminescent properties, *CrystEngComm* 10 (2008) 681–692, doi:[10.1039/b710209g](https://doi.org/10.1039/b710209g).
- [53] Y.-C. Ou, W.-T. Liu, J.-Y. Li, G.-G. Zhang, J. Wang, M.-L. Tong, Solvchromic and photodimerization behaviour of 1D coordination polymer via single-crystal-to-single-crystal transformation, *Chem. Commun.* 47 (2011) 9384–9386, doi:[10.1039/c1cc13018h](https://doi.org/10.1039/c1cc13018h).
- [54] Z. Li, J. Zhou, K. Zhang, Y. Zhang, S. Wu, J. Gong, Playing with isostructural from binary cocrystals to ternary cocrystal solvates of quercetin: tuning colors of pigment, *Cryst. Growth Des.* 22 (2022) 5322–5334, doi:[10.1021/acs.cgd.2c00424](https://doi.org/10.1021/acs.cgd.2c00424).
- [55] H.M.D. Bandara, S.C. Burdette, Photoisomerization in different classes of azobenzene, *Chem. Soc. Rev.* 41 (2012) 1809–1825, doi:[10.1039/C1CS15179G](https://doi.org/10.1039/C1CS15179G).